Biophysical Journal
Article

Biophysical Society

Structural and Dynamic Insights of the Interaction between Tritrpticin and Micelles: An NMR Study

Talita L. Santos,[1] Adolfo Moraes,[2] Clovis R. Nakaie,[3] Fabio C. L. Almeida,[1] Shirley Schreier,[4] and Ana Paula Valente[1,*]

[1]Nuclear Magnetic Resonance National Center, Federal University of Rio de Janeiro, Rio de Janeiro, Brazil; [2]Department of Chemistry, Federal University of Minas Gerais, Belo Horizonte, Minas Gerais, Brazil; [3]Department of Biophysics, Federal University of São Paulo, São Paulo, Brazil; and [4]Department of Biochemistry, University of São Paulo, São Paulo, Brazil

ABSTRACT A large number of antimicrobial peptides (AMPs) acts with high selectivity and specificity through interactions with membrane lipid components. These peptides undergo complex conformational changes in solution; upon binding to an interface, one major conformation is stabilized. Here we describe a study of the interaction between tritrpticin (TRP3), a cathelicidin AMP, and micelles of different chemical composition. The peptide's structure and dynamics were examined using one-dimensional and two-dimensional NMR. Our data showed that the interaction occurred by conformational selection and the peptide acquired similar structures in all systems studied, despite differences in detergent headgroup charge or dipole orientation. Fluorescence and paramagnetic relaxation enhancement experiments showed that the peptide is located in the interface region and is slightly more deeply inserted in 1-myristoyl-2-hydroxy-sn-glycero-3-phospho-1′-rac-glycerol (LMPG, anionic) than in 1-lauroyl-2-hydroxy-sn-glycero-3-phosphocholine (LLPC, zwitterionic) micelles. Moreover, the tilt angle of an assumed helical portion of the peptide is similar in both systems. In previous work we proposed that TRP3 acts by a toroidal pore mechanism. In view of the high hydrophobic core exposure, hydration, and curvature presented by micelles, the conformation of TRP3 in these systems could be related to the peptide's conformation in the toroidal pore.

INTRODUCTION

Although their primary structure is often simple, antimicrobial peptides (AMPs) are a challenge for structural biology because their conformation undergoes complex dynamics that leads to low convergence and geometrical violations in the calculated structures (1,2). This structural diversity is likely related to their interaction with membranes and their mechanism of action; thus, understanding their dynamic behavior can assist in the strategic design of new active molecules (3,4). These peptides are usually short and cationic and acquire an amphipathic conformation upon interaction with the cell membrane. They are under intense scrutiny due to their importance for pharmacological applications (5,6).

The mechanism of action of AMPs is an intensely researched and complex field. The first step of this process is peptide binding to the membrane. Several models have been proposed for the AMP mechanism of action at the membrane level. Three of these, the barrel-stave, carpet, and toroidal pore models, are often considered to explain membrane permeabilization (7–9).

In an attempt to understand their interactions with biomembranes, AMP structures were determined by NMR, both in solution and in the presence of interfaces (10–12). AMPs frequently convert between different conformations in solution, acquiring more stable conformations upon binding to interfaces (1,13–19). NMR is a powerful technique for studying such dynamic systems (1,10). The nuclear Overhauser effect (NOE) can be used to calculate the structure of AMPs, whereas chemical-shift changes and paramagnetic effects can be used to evaluate interactions with interfaces (1,20,21). Furthermore, dynamics can be addressed using relaxation parameters (10).

In NMR experiments, due to size limitations, AMP structures are typically studied in complex with micelles. Due to their smaller size compared to vesicles, these aggregates generally tumble fast in the NMR timescale, yielding narrow lines that are adequate for spectral analysis (22). Micelle-forming detergents provide amphipathic environments similar to those found in lipid bilayers and biomembranes. Micelles have different shapes and sizes

Submitted June 30, 2016, and accepted for publication October 27, 2016.

*Correspondence: valente@cnrmn.bioqmed.ufrj.br

Shirley Schreier and Ana Paula Valente contributed equally to this work.

Editor: Francesca Marassi.

http://dx.doi.org/10.1016/j.bpj.2016.10.034

determined by the chemical nature of their headgroups and the length of their hydrophobic tails (23,24). Physicochemical conditions such as temperature, solutes, and concentration can also affect micellar structure and eventually influence the conformation of bound proteins or peptides, especially the latter. In addition, in view of their size, micelles present pronounced curvature, which distinguishes them from bilayers and may affect the interface properties and play a role in their interaction with different solutes, and, in the case of peptides, in their conformation.

The AMP tritrpticin (VRRFPWWWPFLRR (TRP3)) has broad antimicrobial activity against Gram-positive and Gram-negative bacteria and some fungi (25). Three sequential tryptophan residues (WWW-F motif) flanked by two prolines and four arginines render this peptide unique. These residues are important for interaction with membranes and for the TRP3 mechanism of action (26,27). Yang et al. (25) found that TRP3 recognized its targets with high specificity and efficiency while displaying low hemolytic activity.

TRP3 exists as an ensemble of conformations in solution (13). NMR analyses indicate at least four observable conformations, since four peaks can be assigned to each residue; there are 12 peaks in the Trp indole region instead of the expected three, one for each tryptophan. However, one major conformation is stabilized in the presence of micelles (13,28). The structures of TRP3 and its analogs were determined in the presence of sodium dodecyl sulfate (SDS) and dodecylphosphocholine (DPC) micelles; a turn-turn structure was found in the peptide's C-terminal portion, encompassing the WWW-F motif, with a clustering of the tryptophan side chains (13,28,29). Even in the presence of membrane interfaces, the arginine residues (C- and N-terminal regions) did not converge in the structure calculation, which is consistent with regions in conformational exchange. Experiments in the presence of the spin label 5-doxyl stearate indicated that the peptide is located near the micelle surface, with the aromatic side chains equally partitioned into the hydrophilic-hydrophobic interface. Fluorescence studies making use of the soluble fluorescence quencher acrylamide corroborated these results (13).

The interaction of TRP3 with model membranes—micelles, monolayers, and bilayers—has been studied by means of different techniques. While the average environment of TRP3 in bilayer vesicles of variable lipid composition was determined from measurement of the wavelength of maximal fluorescence emission and red edge effects, insertion of TRP3 into the vesicles was examined using tryptophan fluorescence quenching with both soluble acrylamide and nitroxide-labeled phospholipids, as well as by chemical modification of the tryptophan residues with N-bromosuccinimide. The tryptophan side chains were found to be positioned mostly near the membrane-water interface; these residues appeared to be more deeply inserted in vesicles containing the negatively charged phosphatidylglycerol headgroup (14). In monolayer studies, the peptide was found to interact with phospholipids carrying negatively charged headgroups, but not with zwitterionic phospholipids. Moreover, it displayed specificity toward the phosphatidylglycerol headgroup, abundant in bacterial membranes (30), which could be related to AMP selectivity for prokaryotic cells.

With regard to its mechanism of action, Schibli et al. (14) suggested that TRP3 may act via toroidal pore formation. In a study using planar lipid bilayers, electrical measurements showed that TRP3 has ion-channel-like activity (30). Nevertheless, since the peptide is too short to form a typical pore as in the barrel-stave model, the authors suggested that it acts by means of a toroidal pore mechanism (30), a transient pore formed by a mixture of peptide and lipids that does not require bilayer spanning by the peptide. Vesicle leakage data also suggested that membrane permeabilization occurred at least partly by a toroidal pore mechanism (28).

In studies comparing micelles and bilayers, Bozelli et al. (17) found that the circular dichroism (CD) spectra of TRP3 differed in both environments. Micelles consisting of lysophospholipids with variable headgroup composition were compared to phospholipid bilayers with the same headgroup compositions; therefore, the two systems differed solely in the fact that whereas the former compounds carry a single acyl chain, the latter carry two. Based on the fact that the toroidal pore model implies the formation of positive curvature in the bilayer (8,9), the authors suggested that micellar structures could be envisioned as models of peptide and lipid organization in toroidal pores and that the conformation found for the peptide in micelles resembles that acquired in such pores.

The aim of this work was to contribute to the understanding of TRP3 interaction with micellar interfaces and to characterize the peptide's dynamic behavior in this process. Our study focuses on TRP3 accommodation at the hydrophilic/hydrophobic interface of micelles and subsequent events. The structure and dynamics of TRP3 were examined in the presence of micelles of different chemical nature: zwitterionic (lysolauroylphosphatidylcholine 1-lauroyl-2-hydroxy-sn-glycero-3-phosphocholine (LLPC), n-dodecylphosphocholine (DPC), and N-dodecyl-N,N-(dimethylammonio) butyrate (DDMAB), anionic 1-myristoyl-2-hydroxy-sn-glycero-3-phospho-(1′-rac-glycerol) (LMPG), and nonionic (octylglucoside (OG)) (23,24,31–35). The conformational ensemble was evaluated during detergent titration and it was found that the peptide interacts via conformational selection. Chemical-shift and NOE analyses suggested that TRP3′s structure was similar in all systems, in agreement with the work of Bozelli et al. (17). Our results revealed the imperative constraint of the WWW-F motif for the TRP3 structure acquired at interfaces and showed that pre-organization in the free state is crucial for membrane interaction. Furthermore, it was found that the peptide is slighly more deeply inserted in negatively charged (LMPG) than in zwitterionic (LLPC) micelles.

Finally, since micelles present high hydrophobic core exposure, hydration, and curvature, it is proposed that the

results could be related to the structural and dynamic features of TRP3 in the toroidal pore and that micelles can be envisioned as good models for peptide and lipid molecular arrangement in toroidal pores. It is also pointed out that results found for peptide conformation in micelles may not be straightforwardly applicable to bilayers.

MATERIALS AND METHODS

Reagents

LLPC, LMPG, and DPC were purchased from Avanti Polar Lipids (Alabaster, AL). DDMAB and OG were from Sigma-Aldrich (St. Louis, MO). All detergents were used as received. Acrylamide was from Bio-Rad (Hercules, CA), and the probe gadolinium-diethylenetriamine pentaacetic acid-bismethylamide (Gd(DTPA-BMA)) was purchased from GE Healthcare (Little Chalfont, United Kingdom) and used as received.

Peptide synthesis

TRP3 was synthesized manually using solid-phase methodology (36) with fluorenylmethyloxycarbonyl chloride (Fmoc)-protected amino acids; the synthesis was performed as described by Amblard et al. (37) and Chan and White (38). TRP3 was purified using reverse-phase high-performance liquid chromatography (HPLC) until $> 95\%$, and the mass was checked by matrix-assisted laser desorption ionization-time of flight (MALDI-TOF) mass spectrometry (theoretical m/z = 1901.28; found, 1901.3). All reagents were purchased from Iris Biotech (Santa Clara, CA), except for amino acids (LC Sciences, Houston, TX). For labeled TRP3, the above methodology was applied using ^{15}N-labeled leucine (Sigma-Aldrich).

H-NMR titration

NMR samples were prepared by dissolving 2 mg of TRP3 in 9:1 (H_2O/D_2O) in 500 μL to yield a final concentration of 2 mM. A stock solution of each detergent (LLPC, LMPG, DPC, DDMAB, and OG) was prepared by dissolving the appropriate amount in milli-Q water (Millipore, Billerica, MA) to obtain a final concentration of 0.25 M, with pH between 4.5 and 5.0.

NMR spectra were acquired on a Bruker (Billerica, MA) 800 MHz spectrometer equipped with a TXI 5 mm triple-resonance probe. Spectra were acquired using the solvent suppression scheme Watergate 3-9-19 (Bruker pulseprog p3919gp). One-dimensional (1D) ^{1}H spectra were first acquired in aqueous solution. Then, aliquots of detergent stock solutions were added to achieve the desired final concentration. In all NMR experiments, temperature and pH were maintained at 298 K and between 4.5 and 5.0, respectively.

Chemical shift assignment

Samples containing 2 mM TRP3 in the presence of 13.5 mM LLPC, 15 mM LMPG, 100 mM DPC, 30 mM DDMAB, or 50 mM OG, and 10% D_2O in milli-Q water at pH 4.5 were analyzed by two-dimensional NMR (2D-NMR) experiments. The temperature was maintained at 298 K.

2D ^{1}H NMR spectra were acquired on Bruker 800 or 600 spectrometers equipped with a TXI 5 mm triple-resonance probe. The mixing times were 300 ms for all nuclear Overhauser enhancement and exchange spectroscopy (NOESY) spectra and 80 ms for all total correlation spectroscopy (TOCSY) spectra with 1.2 s of recycle delay. Water suppression was performed using a Watergate 3-9-19 pulse sequence for all TOCSY and NOESY spectra. The number of data points in the F2 and F1 dimensions was 8192 and 512, respectively. The data were processed using NMRPIPE (39). Chemical shift assignment and NOE peak list generation were performed using the NMRView 4.1.3 (40) software package. The assignment of chemical shifts was performed using the method developed by Wüthrich (41).

Proton T_1 experiments

Samples containing 2 mM TRP3 in the presence of 13.5 mM LLPC or 15 mM LMPG, and 10% D_2O in milli-Q water at 298 K, pH 4.5, were analyzed on a Bruker Avance III 600 MHz spectrometer equipped with a TXI 5 mm triple-resonance probe.

Proton T_1 relaxation times were obtained from a series of ^{1}H 2D-NOESY spectra with saturation recovery delays of 100, 200, 300, 400, 500, 750, 1000, and 1500 ms, as reported by Respondek et al. (20). The mixing time for all spectra was 300 ms with 1.6 s of recycle delay. Water suppression was performed using a Watergate 3-9-19 pulse sequence. The number of data points in the F2 and F1 dimensions was 4192 and 300, respectively. The data were processed using the TopSpin software package (Bruker). Subsequently, the peak intensities were fitted to Eq. 1,

$$I = I_o\left(1 - e^{\left(-\frac{t}{T1}\right)}\right), \quad (1)$$

to obtain the relaxation times T_1. I_0 and I are the peak intensities without and with the time of recovery delays (t), respectively.

^{15}N-Leu^{11} dynamic experiments

Samples were prepared using 2 mM of ^{15}N-L^{11} TRP3 and an appropriate amount of detergent to achieve final LLPC (13.5 mM) and LMPG (15 mM) concentrations and 10% D_2O. Milli-Q water was used in all experiments instead of buffer and the pH was adjusted to 4.5. Experiments were performed at 298 K.

A set of ^{1}H-^{15}N heteronuclear single-quantum correlation (HSQC) spectra were recorded on a Bruker 700 MHz spectrometer equipped with a TXI 5 mm triple-resonance probe. Chemical shift assignment and NOE peak list generation were performed using TopSpin software (Bruker). ^{15}N T_1 and ^{15}N T_2 relaxation times were measured from spectra with different relaxation delays: 50, 100, 200, 300, 400, 600 (triplicate), 800, 1000, and 1500 ms for T_1 and 16.96, 33.92, 50.88, 84.80 (triplicate), 118.72, 152.64, 169.60, and 203.52 ms for T_2. The errors in the peak intensities were calculated from triplicate experiments. The ^{1}H-^{15}N heteronuclear NOEs were determined from the ratio of peak intensities with and without saturation of the amide protons. Errors in the heteronuclear NOE values were calculated from peak intensities and noise levels in reference and saturated spectra. We used 4, 2, or 6 s of recycle delay for T_1, T_2, or heteronuclear NOE measurements, respectively.

Paramagnetic relaxation enhancement

To obtain paramagnetic relaxation enhancement (PRE), a 2 mM TRP3 solution in the presence of 14 mM LLPC or 15 mM LMPG was titrated (1, 2, 3, 4, and 7 mM) with the gadolinium-based paramagnetic relaxation agent Gd(DTPA-BMA), purchased from GE Healthcare. Proton T_1 relaxation times were obtained by fitting the measured intensities to Eq. 2 at each concentration of Gd(DTPA-BMA). Then, the proton T_1 relaxation times were fitted linearly as a function of Gd(DTPA-BMA) concentration and the linear coefficient for each residue was extracted and used to create a plot of PRE versus residue number (20).

Experimental PRE values for TRP3 in the presence of LLPC and LMPG micelles were fitted to the equation described by Respondek et al. (20),

$$\begin{aligned} PRE = {} & (\kappa\pi/6)\{A + 1.5\sin[\tau(x-1)] \\ & - \cos(\tau)B\cos[1.745(x-1)+\rho]\}^3 \end{aligned}, \quad (2)$$

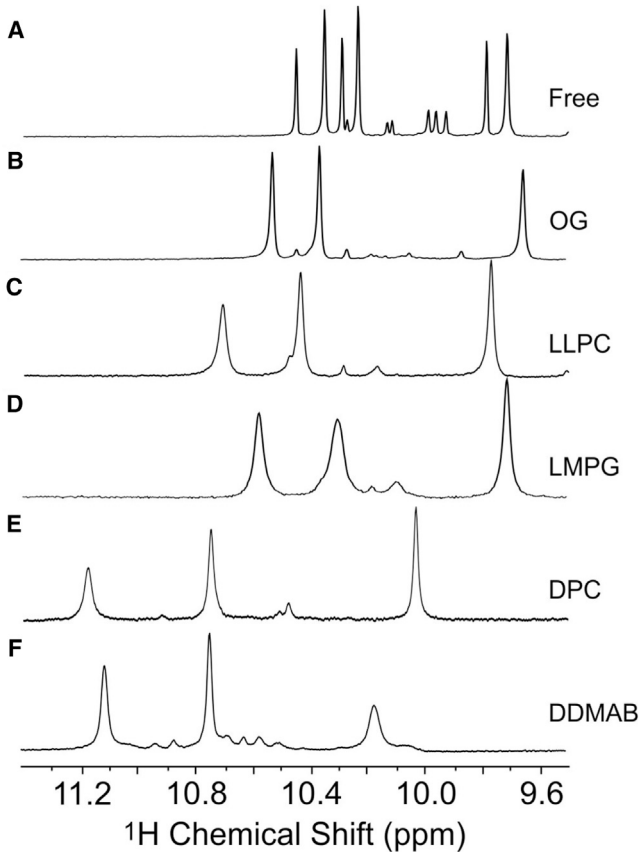

FIGURE 1 TRP3 conformation ensemble. NH indole region of 1D-NMR spectra in the absence (*A*) and presence (*B–F*) of micelles. The micelle concentrations used were (*B*) 50 mM OG, (*C*) 13.5 mM LLPC, (*D*) 15 mM LMPG, (*E*) 100 mM DPC, and (*F*) 30 mM DDMAB. The three intense peaks in the presence of detergents mean that a major structure was stabilized. The higher, intermediate, and lower chemical shift peaks were attributed to W_6, W_7, and W_8, respectively. Spectra were collected in a Bruker 800 MHz spectrometer.

where τ is the tilt angle, ρ the azimuth angle, A the immersion depth of the helical axis at the position of the N-terminal residue, and B the helix radius (3.25 Å for Hα); κ is a constant that combines several basic magnetic constants with the concentration of paramagnetic probe; and x is the residue number in the primary sequence. Fitting of Eq. 2 (2) to the experimental PRE values was done using the Levenberg-Marquardt algorithm optimizing four different variables: κ, A, ρ, and τ.

Fluorescence experiments

Sample preparation

TRP3 stock solutions were prepared by dissolving the peptide in water up to an optical density of 0.05 at 280 nm (~18 μM). These solutions were also used to dissolve detergent and acrylamide, avoiding sample dilution.

Tryptophan fluorescence

Experiments were carried out on an Agilent Tech Cary Eclipse fluorescence spectrophotometer equipped with single-cell Peltier for temperature control and a 1 cm path length cuvette. Scans were run at 298 K with the following experimental parameters: excitation wavelength of 280 nm; emission detection from 300 to 400 nm; 5 nm slit width for excitation and 2.5 nm for emission; and scan speed of 5 nm/s. Each experiment was repeated 10 times to obtain an average curve.

Fluorescence quenching by acrylamide

Experiments were performed under the same conditions as above. A 4 M acrylamide stock solution was used for titration in the concentration range 0–0.2 M. Stern-Volmer constants (42) were determined using the equation

$$I_0/I = 1 + K_{SV}[Q], \quad (3)$$

where I_0 and I are the fluorescence intensities in the absence and presence, respectively, of variable acrylamide concentrations, K_{SV} is the Stern-Volmer constant, and [Q] is the acrylamide concentration.

RESULTS

TRP3 has multiple conformational states in solution due to isomerization of the two prolines adjacent to the WWW motif (13,28). These states can be monitored by evaluating the HN indole region of the 1D-NMR spectrum, because it presents 12 peaks instead of three (i.e., one for each tryptophan residue). The presence of these peaks indicates a slow exchange regime between conformations in the chemical-shift timescale (43), rendering it possible to study the ensemble of the TRP3 peptide conformations by NMR.

Fig. 1 shows the indole region of the ^{1}H 1D spectra used as an indicator of conformational changes. In the absence of detergents, 12 peaks were observed (Fig. 1 *A*). The spectra in Fig. 1, *B–E*, were obtained at the highest detergent concentration used. As previously reported, addition of detergents stabilized a major conformation and the spectra presented three predominant intense peaks with larger chemical shift dispersion. However, minor peaks were still observed. Although each tryptophan exhibited a different chemical shift, their appearance in the spectrum was always in the order W^6, W^7, and W^8, from the lower to the higher field.

Furthermore, the chemical shifts obtained for TRP3 in the presence of micelles were very similar in OG, LLPC, or LMPG, whereas distinct values were obtained in the presence of DPC and DDMAB micelles. Since OG, LLPC, and LMPG carry hydroxyl groups in the polar headgroups, it is conceivable that their ability to form hydrogen bonds with the peptide's backbone, as well as with different residues, in particular arginines (44), could play a role in the observed chemical shift differences.

Another clear difference between the spectra in Fig. 1 refers to the line width. Table 1 shows how the spectral line widths measured for the indole peak vary depending on detergent chemical nature, with TRP3/OG yielding the narrowest line widths, followed by TRP3/DPC, TRP3/LLPC, and TRP3/DDMAB, and TRP3/LMPG presenting much larger line widths. It is widely known that this spectral feature is related to relaxation properties (T_2), i.e., to the system's tumbling rate, which in turn is a function of micellar size. Table 1 also displays values of monomer

TABLE 1 Line Width of Indole Hydrogen Peaks and Properties of the Micellar Systems

	W^6	W^7	W^8	Average Line Width	Monomer MW	Micelle N_{agg}	Average Micelle MW × 10^3[a]	Micelle + TRP3 MW × 10^3[b]	Micelle + TRP3 τ_{app} (ns)[c]
OG	11.4	11.4	13.9	12.2	269	27[d,e]	7.9	11.7	5.5
						90[e,f,g]	26.3	30.2	12.2
LLPC	24.4	20.9	17.4	20.9	439	78[h]	34.2	56.8	21.3
						55[i]	24.1	46.7	17.9
LMPG	30.0	40.7	22.2	31.1	478	55[d]	26.3	43.5	16.8
DPC	26.4	19.4	15.7	20.5	351	60–80[d]	24.6	30.0	12.1
DDMAB	21.2	19.1	40.1	26.9	300	47[f,j]	14.1	21.1	9.0

The indole NH corresponds to aromatic Hε. Line width values are given in Hertz. Resonance assignment was performed using TOCSY and NOESY experiments. MW, molecular weight; N_{agg}, aggregation number

[a]Approximate micelle MW using the average N_{agg}.

[b]Micelle MW estimated assuming that the peptide is fully bound.

[c]Apparent rotational correlation time calculated using the Stokes-Eisntein equation and the micelle MW estimated assuming a fully bound peptide.

[d–j]N_{agg} values were taken from (23)[d], (32)[e], (34)[f], (47)[g], (35)[h], (48)[i], and (33)[j].

molecular weight, aggregation number (N_{agg}), micelle molecular weight calculated based on N_{agg} (in the absence and presence of peptide, assuming that the peptide is fully bound), and rotational correlation times of the micelle-TRP3 complex. There is not a very good agreement between line-width variation and the size-related micellar physical properties. However, it should be mentioned that a survey of the literature indicates a large scatter of these values. In addition, it should be considered that peptide binding could have modified these properties. All these uncertainties prevent us from drawing quantitative conclusions about the correlation between the line widths and micellar size. Furthermore, according to Lauterwein et al. (45), a variety of motions—micelle overall motion, motion of the peptide within the micelle, and motion of the hydrophobic chains within the micelle—could contribute to the observed line widths. Such complexity prevents us from deconvoluting all contributions using only the indole 1D spectrum; further data are needed to fully understand the process.

In addition, the dynamics of the bound peptide is also probably influenced by different interactions with the different headgroups. This seems to be particularly evident when analyzing the effect of headgroup on the spectral line width for the LMPG-bound peptide. This is the only case where electrostatic interactions contribute to binding; therefore, these interactions should play an important role on peptide dynamics at the micelle interface. These dynamic effects are also probably responsible for the observed differences between the different tryptophan HN indole peaks in a given system. It is important to mention that there is no indication of a significant amount of free peptide in the spectra.

The major TRP3 structure in the different micelles

To determine the major structure in each system, TOCSY and NOESY experiments were performed at detergent concentrations where no changes in chemical shifts were observed upon increase in concentration. As shown in Fig. 2, the NOESY spectra exhibited good line width and dispersion, which allowed for the unambiguous assignment of ~90% of the resonances. These data were compared with the spectra obtained by Schibli et al. (13,28) for TRP3 and its analogs bound to SDS and DPC micelles.

As reported by Schibli et al. (13,28), TRP3 adopts two successive turns in the C-terminus induced by the two proline residues, the N-terminus being more extended. Additionally, the presence of NOEs between the Hδ of the prolines and the Hα and Hβ of the preceding residues indicates that the prolines are in a *trans* configuration. We found the same NOE pattern for the proline residues in all micellar systems, indicating that binding to the different micelles also stabilized the *trans-trans* isomer.

A comparison of the spectra indicated that the chemical shifts were very similar in all micellar systems. Fig. 3 shows

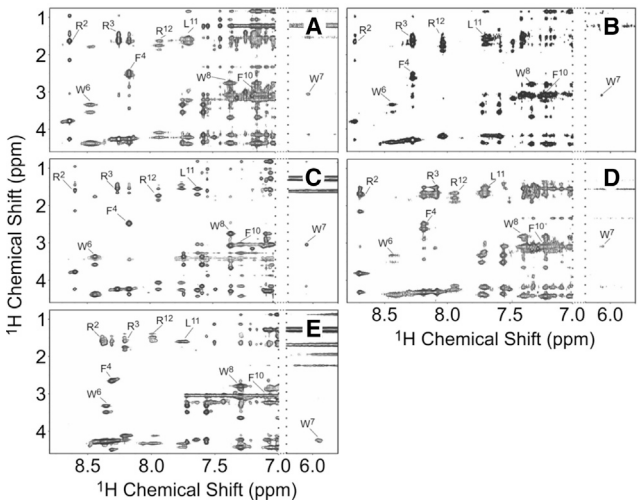

FIGURE 2 TRP3 resonance assignment. The amidic region of the NOESY spectra of 2 mM TRP3 is shown in the presence of (*A*) 13.5 mM LLPC, (*B*) 100 mM DPC, (*C*) 50 mM OG, (*D*) 15 mM LMPG, and (*E*) 30 mM DDMAB at 298 K (pH 4.8). The NH of W7 was found around 6 ppm in all spectra. All chemical shifts of the peptide hydrogens are similar, independent of micelle nature.

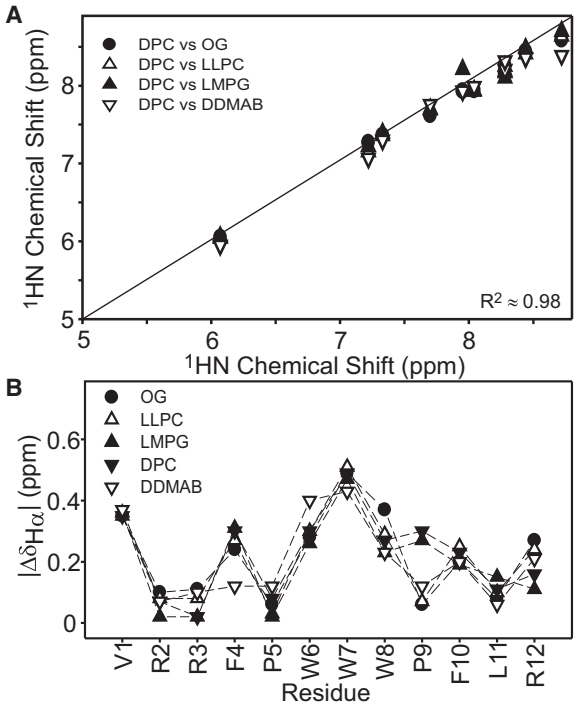

FIGURE 3 Comparison of TRP3 chemical shifts in different micelles. (*A*) Correlation between the peptide HN chemical shifts in DPC and those in LLPC, LMPG, DDMAB, and OG. (*B*) Difference between the Hα chemical shifts in different micelles and random coil values, as reported by Wishart (46).

a comparison of the amidic and Hα hydrogens in the different systems as a function of residue number. The data demonstrate that the chemical shift values are similar, independent of micellar nature. Because the chemical shift reflects the chemical environment of each nucleus (46), it is plausible to propose that the TRP3 backbone structure is similar in all aggregates. Another indication of structural similarity is the resemblance of the NOE patterns observed in all micellar systems (Fig. S1). The medium-range NOEs ((i, i + 2) and (i, i + 3)) indicate a similar backbone behavior. These results are in agreement with those of Bozelli et al. (17), who found similar CD spectra for TRP3 in the presence of different types of micelles.

Pathway for structural TRP3 stabilization

Fig. 4 presents the effect of increasing detergent concentrations on TRP3's 1D ^{1}H NMR spectra. The titration curves were analyzed based on changes observed for the indole peaks. The spectra are complex, displaying changes in chemical shifts, as well as considerable broadening of some lines.

Fig. 5 shows that increasing detergent concentrations caused continuous changes of the chemical shifts. The colored circles indicate a probable trajectory of the resonances from the initial to the final state. However, this trajectory is just a suggestion, as it is difficult to follow each peak unambiguously. It is worth noting that the changes in chemical shifts started at, or approximately at, the critical micellar concentrations (CMCs, in mM) of the detergents (OG, 18–20 (23,32,47); LLPC, 0.4–0.9 (35,48); LMPG, 0.16 (23,49); DPC 1.5 (23,24,34,50); and DDMAB, 4.3 (33,34,51)). Line broadening can be seen at intermediate detergent concentrations (Fig. 4), when samples contained higher peptide/micelle ratios. In these cases, most likely, the exchange between free and micelle-bound peptide contributes to the spectral features. In addition, aggregates different from the final micelle-peptide system are also likely to be formed. This is clearly suggested by the spectral changes at detergent concentrations below, or at, the CMC, as is the case with OG and LLPC (Fig. 4, *A* and *B*). The most dramatic effect occurs in the case of DDMAB (Fig. 4 *E*), whose CMC is 4.3 mM (34,51). At 5.0 and 6.0 mM, the detergent is essentially monomeric, whereas at 10.0 mM about half of it should be in the micellar form. It is conceivable that the observed spectra contain contributions of the equilibria between different states of the peptide: free, micelle-bound, and in aggregates with different peptide/detergent stoichiometry. These data indicate that the peptide is capable of promoting aggregation of monomeric detergent, possibly via interaction between peptide and detergent hydrophobic portions.

At the end of the titration, the final structure was attained, as indicated by the presence of three primary indole peaks. The final line widths were broader than those in solution because of the formation of the TRP-micelle complex, as mentioned above. Moreover, the movement of peaks in the titration experiments provided interesting insights into the changes in the conformational ensemble (Fig. 5). Assuming that the suggested trajectories are reasonable, the peaks labeled with the blue circle appear to change only slightly during titration, while the peaks labeled with orange and purple circles changed more. The trajectories were clearly observed in the OG system (Figs. 4 *A* and 5 *A*), where the three peaks could easily be traced, most likely because the interface is not charged, the micelle size is small, and the final chemical shifts were not very different from those of the initial state.

Our results suggest that the final conformation (or a similar one) found in each micelle could already be present in the initial ensemble. Therefore, we propose that TRP3 interacts with the micelles via conformational selection, i.e., the bound conformation is already present in the free ensemble and the equilibrium between conformations is re-established upon binding (52–56).

Analysis of TRP3 dynamics by means of relaxation parameters

We measured TRP3 relaxation parameters in solution and in the presence of LLPC and LMPG micelles. These micelles were chosen based on the proposal by Bozelli et al. (17) that

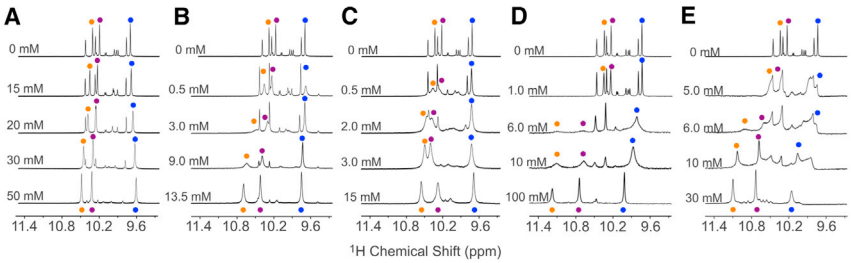

FIGURE 4 Changes in ensemble structure upon interaction of TRP3 with different detergents. Shown is the NH indole region of the 1D ^{1}H spectra upon titration with (*A*) OG, (*B*) LLPC, (*C*) LMPG, (*D*) DPC, and (*E*) DDMAB. All spectra were recorded at 298 K (pH 5.0). The colored circles indicate Hε of W^{6} (*orange*), W^{7} (*purple*), and W^{8} (*blue*) according to the chemical shift assignment of 2D-NMR spectra at the highest detergent concentrations. The intensities were normalized to facilitate visualization. Fig. S2 shows the spectra during titration with LMPG without normalization. To see this figure in color, go online.

their use allows mimicking the headgroup composition of biological membranes. PC is one of the major phospholipids in the outer leaflet of mammalian membranes and PG is one of the main phospholipids in the outer leaflet of bacterial membranes (57).

The dynamic profile of TRP3 can be determined by relaxation experiments. Therefore, we measured the longitudinal relaxation parameters (T_1) for both systems. T_1 values were measured using 2D-NOESY spectra, where the delay between presaturation and the start of the NOESY sequence was varied between 100 and 1500 ms. The intensity of the α-protons was monitored as a function of these delays. The T_1 values obtained as a function of residue number are shown in Fig. 6. Not all residues were properly measured because of overlap in Hα resonances, as was the case for the V^{1}, P^{5}, and P^{9} residues, or because of line broadening, as was the case for W^{7}. The results revealed that TRP3 presented similar T_1 values for all measured residues, suggesting that in LLPC or LMPG micelles, the relaxation parameters are dominated by micelle tumbling. However, the slightly smaller values observed for residues R^{2}, R^{3}, and F^{4} were attributed to a greater flexibility in this region. Moreover, the tryptophan residues, as well as F^{10}, exhibited higher T_1 values, indicative of higher τ_c values and therefore stronger interaction with the micelles (Fig. 6).

The free TRP3 conformations were very difficult to evaluate using ^{1}H relaxation parameters because of the inherent ambiguity in their assignment. Therefore, TRP3 was labeled with ^{15}N-L^{11} and T_1, T_2, and heteronuclear NOE experiments were performed for ^{15}N. Because TRP3 presents four conformations, the ^{15}N labeling of L^{11} yielded four peaks in the HSQC spectrum (Fig. S3). Table S1 shows the relaxation parameters for the four observed peaks, representing all four conformations. The HN coupling constants were also measured, but no significant differences were observed. ^{15}N-L^{11}-TRP3 was also investigated in the presence of LLPC and LMPG micelles (Table S1). When compared to the free state, the relaxation parameter values changed substantially as a result of peptide-micelle interaction. In addition, the comparison between T_2 values for LLPC and LMPG shows that these values are lower in the latter case, suggesting that TRP3 interacts to a somewhat larger extent with LMPG, yielding a higher τ_c value.

For a more quantitative analysis of TRP3-micelle interactions, we monitored the effect of adding Gd(DTPA-BMA) on the ^{1}H NMR relaxation. Gd(DTPA-BMA) is an inert, water-soluble, paramagnetic compound that displays no specific binding to micelles or peptides (20,58). In solution, this compound enhances the relaxation rates of nuclei exposed to solvent through PRE. The PRE values were obtained by monitoring proton longitudinal relaxation rates in the presence of increasing Gd(DTPA-BMA) concentrations (Fig. 7 *A*). The longitudinal relaxation rates, R_1, were calculated from a set of eight saturation-recovery 2D-NOESY

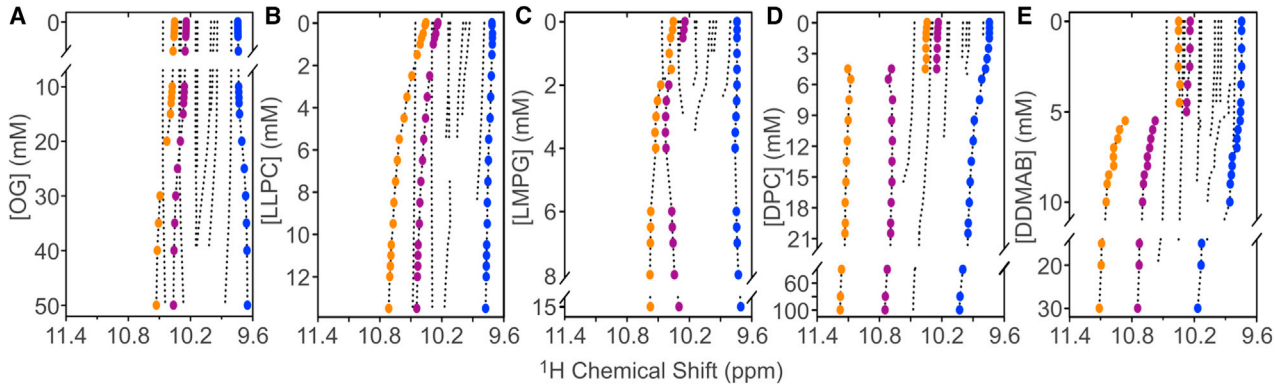

FIGURE 5 Schematic representation of the trajectory of TRP3 Hε resonances as a function of detergent concentration. The changes in chemical shift upon peptide-micelle interaction are indicated by colored circles at all concentrations tested for residues W^{6} (*orange*), W^{7} (*purple*), and W^{8} (*blue*). To see this figure in color, go online.

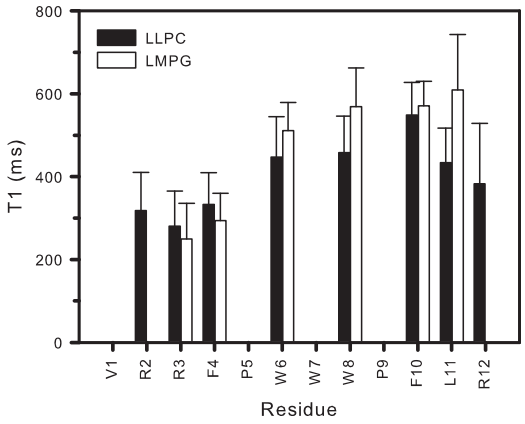

FIGURE 6 $^{1}H\alpha$ T_1 relaxation constants of TRP3 residues at 600 MHz in the presence of 13.5 mM LLPC (*black bars*) and 15 mM LMPG (*white bars*), with a 2 mM TRP3 concentration at 298 K (pH 5.0).

experiments, as described in Materials and Methods. Fig. 7 *B* shows the PRE values of Hα protons as a function of residue number in LLPC and LMPG micelles. Overall, for both types of micelles, the PRE effect was higher for residues R^2, R^3, and F^4 and lower for the WWW-F residues, indicating greater and lesser solvent exposure, respectively, based on the T_1 values measured for Hα (Fig. 6). These results confirm the importance of the WWW-F region for peptide binding to the micelle.

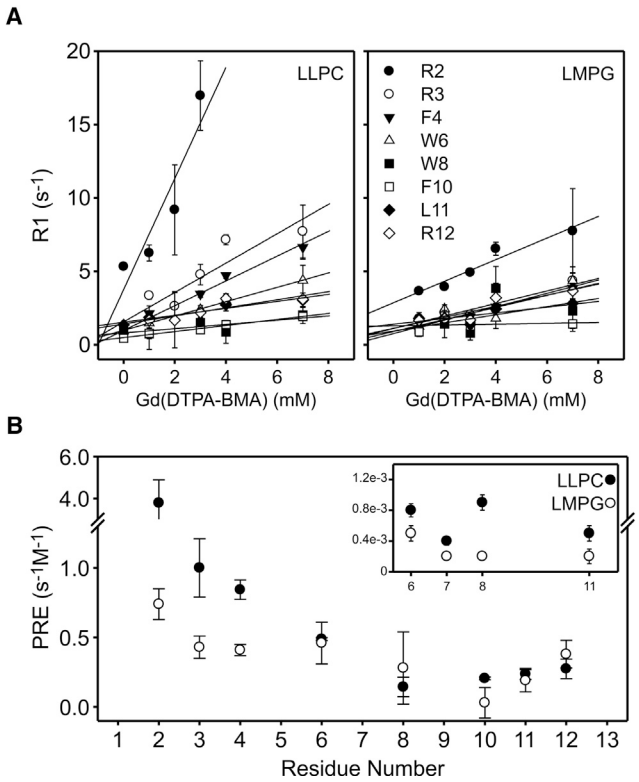

FIGURE 7 (*A*) Effect of Gd(DTPA-BMA) concentration on TRP3 Hα T_1 in the presence of 13.5 mM LLPC (*left*) and 15 mM LMPG (*right*) micelles. (*B*) PRE values as a function of residue number in LLPC (*solid circles*) and LMPG (*open circles*) micelles. The inset shows the values for the tryptophans NHε and for Leu^{11} Hδ obtained as described in Materials and Methods.

TABLE 2 λ_{EM}^{max} of TRP3 Fluorescence Spectra and K_{SV} for Acrylamide Fluorescence Quenching in the Absence and Presence of Micelles

	λ_{EM}^{max} (nm)	$\Delta\lambda_{EM}^{max}$ (nm)	$K_{SV}(M^{-1})$
In solution	356	–	18.2
OG	351	5	7.2
LLPC	346	10	4.0
LMPG	348	8	5.1
DPC	348	8	6.5
DDMAB	349	7	12.8

λ_{EM}^{max}, maximum emission wavelength; K_{SV}, Stern-Volmer constant.

Analysis of peptide location and orientation in the micelles by means of fluorescence and PRE experiments

To assess the pepetide location in the micelles, we examined the quenching of TRP3's intrinsic fluorescence by acrylamide. Table 2 presents the values obtained for maximum emission wavelengths (λ_{em}), as well as Stern-Volmer constants (K_{SV}). As reported in the literature, the decrease in λ_{em} from 5 nm in OG to 10 nm in LLPC micelles when compared to free peptide indicated formation of TRP3/micelle complexes. Similar results were obtained in both micelles and phospholipid vesicles (13,14,17,59). Moreover, significant changes were observed in the Stern-Volmer constants. Fluorescence quenching decreased in the presence of micelles, indicating a decreased exposure to acrylamide. These results are consistent with the localization of the tryptophans at an interfacial region. The K_{SV} values were larger in the case of DDMAB, suggesting that the peptide was more exposed to the aqueous phase. In contrast to the lysophospholipids and DPC, the positive charge in DDMAB's headgroup (the ammonium moiety) is located more to the interior of the interface. It is conceivable that this region would repel the highly positively charged peptide, causing it to be located at a more water-exposed site.

PRE measurements can provide information about the orientation of peptides inserted in micelles (20,58). As proposed by Respondek et al. (20), PRE experimental values can be modeled by Eq. 2 (Materials and Methods) for helical peptides. This equation considers helical peptides immersed in micelles and is written as a function of three variables, the tilt angle (τ), the azimuth angle (ρ), and the immersion depth of the N-terminal residue with respect to the micellar surface. Taken together, these parameters can contribute to the interpretation of the relationship between PRE values and the orientation of the peptides in micelles.

The PRE values of the TRP3 N-terminal residue exhibited one significant difference. The observed PREs were higher in LLPC micelles, suggesting a lesser interfacial insertion than in LMPG micelles. Similar PRE values

were observed in the tryptophan region. Interestingly, the PRE value for F^{10} was also different in both systems. The smaller PRE value, therefore reflecting greater insertion, was observed in LMPG micelles (Fig. 7 *B*). We also analyzed the PRE effect on the side chains of the WWW-L motif (Fig. 7 *B*, *inset*). The results for Hε of the WWW and Hδ of L^{11} were significantly lower than that observed for Hα, suggesting that these residues are inserted more deeply in the micelle.

By fitting Eq. 2 to our experimental PRE values we were able to determine the tilt (τ) and azimuth (ρ) angles for the relative orientation of TRP3 in the two different micelles (Table S2). Based on the structures of TRP3 and its amidated analog determined in SDS and DPC micelles, respectively (13,28), as well as the TRP3/DPC Ramachandran plot (Fig. S4), we assumed that residues F^4–L^{11} have helical character. The tilt angles for TRP3 were $-41.8 \pm 1.2°$ in LLPC and $-35.5 \pm 3.5°$ in LMPG, showing similar peptide orientations in both membrane mimetic systems. However, the calculated depths were different: -1.07 ± 0.3 Å in LLPC vand -2.62 ± 0.2 Å in LMPG micelles. These results suggest that the peptide is more inserted in the LMPG micelles.

In addition, very similar values of azimuth angles were observed in LMPG ($-60.3 \pm 2.2°$) and LLPC ($-56.8 \pm 2.7°$) micelles (Table S2). In both types of micelles, the azimuth angle determines the helix rotation from the micelle surface and corresponds to the orientation of F^4 toward the interior. These results are summarized in Fig. 8. The structure of amidated TRP3 in DPC (PDB: 2I1D) is displayed based on the PRE data. The peptide appears more inserted into LMPG toward the interior of the hydrophobic region of LMPG micelles when compared to LLPC.

Although our results refer to micellar systems, they correlate well with those of Salay et al. (31), who examined the interaction of TRP3 with Langmuir phospholipid monolayers of dipalmitoylphosphatidylcholine, dipalmitoylphosphatidylethanolamine, dipalmitoylphosphatidic acid, and dipalmitoylphosphatidylglycerol. It was found that the peptide interacted to a much larger extent with the negatively charged phospholipids and exhibited specificity toward the PG headgroup.

DISCUSSION

Over millions of years, the driving forces of natural selection and evolution have been related to interactions between proteins and other molecules to perform their functions. Biological processes involve molecular recognition, which requires well-structured molecules able to perform specific tasks but that also exhibit dynamic properties that render them capable of interacting with multiple targets.

TRP3 interacts with micelles via conformational selection

Initially, binding processes were interpreted as "lock-and-key" recognition events where the conformation in solution is optimal for perfect binding (60). The ability to bind to multiple targets led to the idea of an "induced fit" process, which implied that a conformational change occurs upon binding (60–62). In the 1960s, two groups formulated the theory of conformation selection, proposing that the bound conformation was already present in solution (6,61), in equilibrium with different proportions of other conformations (54,61).

Currently, the conformation selection theory has been used to explain several types of interaction, especially in the case of allostery (54–56). The most accepted theory is that with conformational selection, the dominant bonding process occurs in conjunction with structural adjustment (induced fit) to optimize the interaction (63–67).

In this work, we showed that TRP3 interacts with micelles through the conformational selection mechanism, where the bound form is selected from a family of conformations that interconvert slowly in the NMR timescale. Structural diversity is important for the action of TRP3,

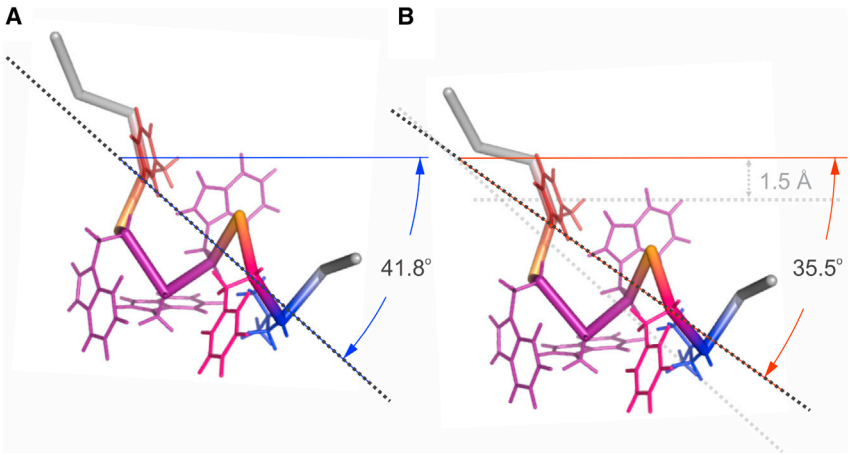

FIGURE 8 Immersion depths and orientation of TRP3 based on PRE results. The NMR calculated structure of C-amidated TRP3 in the presence of DPC micelles deposited in the Protein Data Bank (PDB: 2I1D) represents the results in LLPC (*A*) and LMPG (*B*) micelles. Tryptophan residues are colored purple, phenylalanines pink, leucine blue, and the backbone of proline residues orange. The tilt angle for TRP3 was calculated to be $-41.8 \pm 1.2°$ in LLPC and $-35.5 \pm 3.5°$ in LMPG, showing a similar orientation in both micelles. However, the peptide calculated depth was different: -1.07 ± 0.3 Å in LLPC and -2.62 ± 0.2 Å in LMPG micelles, suggesting that the peptide is more deeply inserted in the latter. To see this figure in color, go online.

allowing it to bind to lipid membranes of different chemical nature.

Structural pre-organization decreases the entropic penalty for the interaction process

Our data suggest that TRP3 presents structural pre-organization in the free state and that this feature is crucial for membrane interaction. Because the interaction of a fully flexible peptide with the membrane leading to a stable conformation implies a considerable decrease in entropy, the pre-organization of flexible ligands increases association constants by decreasing the entropic penalty of the process (68). Related information is being used in medicinal chemistry to design molecules that prefer to adopt a bound structure (68). In fact, this strategy has been successfully applied to HIV protease, BANCE1, and streptomycin (69).

Conformation of TRP3 bound to the micellar systems

The backbone conformation of TRP3 stabilized upon binding is very similar in all micellar systems, regardless of the chemical nature of the detergents headgroups. Although we have not calculated the structure, the chemical shift values of the amide and α-hydrogens were very similar for the different micelle compositions, indicating similar micelle-bound peptide conformations. The similarity of TRP3 conformations and of some of its analogs stabilized by different micellar interfaces has been indicated by NMR, CD, and fluorescence experiments (13,14,17,29,70). Similar results were found for melittin in micelles of various detergentes (45) and for PR-1, a synthetic peptide modeled after the microbicide domains of the platelet microparticle factor-4 family, in SDS and DPC micelles (71).

The micelle-bound conformation of TRP3 can be explained at least in part by the presence of aromatic residues and prolines. The aromatic residues, F^4, W^6, W^7, W^8, and F^{10}, have bulky side chains and their presence in the primary sequence hampers the backbone motion (2). Furthermore, the presence of proline residues (P^5 and P^9) further decreases the flexibility, imposing additional restrictions on the backbone motion. The specific features of amino acid restraint may be illustrated by analysis of their Ramachandran plots. Residues with small side chains, such as glycine, can occupy different regions in the graph (i.e., a larger range of angles). For amino acids with bulky side chains, a lesser number of angles is possible, due to steric hindrance. The Ramachandran plot will vary depending on the amino acid sequence and the secondary structure features of the region.

Stabilization of the aromatic region was observed for PW2, an anticoccidial peptide that has several conformations in solution and acquires a more stable one in the presence of an interface (1,72,73). PW2's calculated structure in the presence of SDS micelles and DPC micelles using NOEs presented a convergent and similar conformation in the two systems. The structures are similar primarily in the aromatic region. The PRE data obtained using an N-terminally modified peptide containing the TOAC amino acid (TOAC-PW2) indicated that PW2 has an ordered aromatic region (YWWR), even in solution. Moreover, molecular dynamics data showed that the aromatic nucleus is found in restricted regions of the Ramachandran plot.

The presence of proline in the primary sequence imposes important constraints on chain movement, and TRP3 has two proline residues flanking the sequential tryptophans (~PWWWP~). Therefore, the aromatic region is even more constricted.

Tryptophan has special features

Tryptophan residues play an important role on the interaction of peptides with membranes (74). A large number of studies on the topology of membrane proteins and peptides shows that tryptophan prefers to reside at the lipid interface. A number of electrostatic interactions appear to contribute to localization, including hydrogen bonding to the lipid carbonyl groups, cation-π interactions (in particular with phospholipid ammonium moieties), interactions between the indole dipole and the lipid bilayer's strong interfacial electric field, and nonspecific electrostatic stabilization (75). Phospholipid phosphate groups have also been implied in hydrogen bonding (76). Yau et al. (77) also pointed out that the preference of tryptophan for the membrane headgroup region is dominated by tryptophan's flat rigid shape, which limits access to the hydrocarbon core, and by its π electronic structure and associated quadrupolar moment (aromaticity), which favor residing in the electrostatically complex interface environment.

In this context, it seems reasonable that the three tryptophans in TRP3 will play an important role in favoring the peptide's interfacial location, and it helps in understanding why the replacement of the tryptophans by phenylalanines favors the ability of this analog to penetrate the membrane, as suggested by Schibli et al. (28). Nevertheless, as discussed by Schibli et al. (13), "the complicated relationships between amino acid composition, sequence, 3D structure, membrane interactions, antimicrobial activity, and hemolytic activity may not be easily explained by simple rules where one specific amino acid or one unique secondary structure is always responsible for a specific characteristic."

The depth of TRP3 insertion depends on headgroup charge

Paramagnetic relaxation experiments evinced that TRP3 is more deeply inserted in negatively charged LMPG micelles

than in zwitterionic LLPC micelles. These data are in agreement with those found for lipid bilayers (14).

Tritrpticin interaction with highly curved micellar systems—significance of this process for the peptide's mechanism of action

The available data obtained thus far, both by NMR (13,28) and by CD (17) experiments, suggest that TRP3 acquires similar conformations in micellar systems of variable chemical composition. The data presented here corroborate these findings and add a list of new, to our knowledge, micelle-forming compounds that promote acquisition of a similar conformation by TRP3. Clearly, the P^5WWWP^9 sequence imposes considerable constraints on TRP3's conformation; thus, it is plausible that the propensity of the peptide to acquire the observed conformation prevails over the eventual effects of different peptide-micelle interactions on the peptide structure. As shown by the results, the different chemical nature of the detergents does lead to differences in observed properties; however, they do not affect TR3's conformation to a significant extent.

The relationship between non-lamellar phases and the mechanism of action of AMP and the role of lipid curvature in peptide-membrane interaction have been discussed in reviews by Haney et al. (78) and Koller and Lohner (79), respectively. We have previously proposed that micellar systems provide positive curvature that can be regarded as mimicking the curvature in toroidal pores, and we suggested that the conformation found for TRP3 in micelles represents that of the peptide in the toroidal pore (17). In this context, the results presented here contribute to the understanding of the mechanism of action of the peptide at a molecular level.

CONCLUSIONS

In conclusion, this work has shown that the antimicrobial peptide tritrpticin binds to micelles, irrespective of whether their forming compounds contain neutral, zwitterionic, and negatively charged headgroups, and irrespective of the orientation of the headgroup dipole. The data also indicated that the TRP3-micelle interaction occurs via conformational selection and that the backbone conformation stabilized upon binding is very similar in all micellar systems, regardless of the chemical nature of the detergent headgroups. We also corroborated previous data that showed that the peptide is located in the region of the membrane-water interface, and we discuss that the presence of three tryptophan residues contributes to this location. Moreover, PRE experiments provided evidence for a greater depth of peptide penetration in negatively charged micelles.

Based on these findings and on the topographical similarity of micelles and toroidal pores, we propose that peptide-micelle systems can be used to mimic the molecular organization of peptide and lipid in the toroidal pore and that the conformation acquired by the micelle-bound peptide could resemble that acquired by the peptide in the pore. Finally, it is important to recall that, due to experimental restrictions, a large amount of peptide structure determination by NMR is performed using micelles. However, due to the differences between the bilayer and micelle environments, the structure found in the latter may not always correspond to that present in bilayers.

SUPPORTING MATERIAL

Four figures and two tables are available at http://www.biophysj.org/biophysj/supplemental/S0006-3495(16)30993-6.

AUTHOR CONTRIBUTIONS

A.P.V., S.S., F.C.L.A., T.L.S., A.M., and C.R.N. designed research; T.L.S. and A.P.V. performed research; T.L.S. and C.R.N. synthetized and purified TRP3; T.L.S, S.S. and A.P.V analyzed data; and T.L.S., S.S. and A.P.V. wrote the article.

ACKNOWLEDGMENTS

We thank Dr. J. C. Bozelli, Jr., for careful reading of the manuscript and helpful suggestions.

T.L.S. acknowledges receipt of a PhD fellowship from Conselho Nacional de Desenvolvimento Científico e Tecnológico (CNPq); A.P.V. acknowledges receipt of a research grant from CNPq and Fundação de Amparo à Pesquisa do Estado do Rio de Janeiro (FAPERJ); A.P.V., S.S., F.C.L.A., and C.R.N. are recepients of CNPq research fellowships; and A.P.V. and F.C.L.A. are recipients of FAPERJ research fellowships.

REFERENCES

1. Gomes-Neto, F., A. P. Vente, and F. C. L. Almeida. 2013. Modeling the interaction of dodecylphosphocholine micelles with the anticoccidial peptide PW2 guided by NMR data. *Molecules.* 18:10056–10080.
2. Valente, A. P., C. A. Miyamoto, and F. C. L. Almeida. 2006. Implications of protein conformational diversity for binding and development of new biological active compounds. *Curr. Med. Chem.* 13:3697–3703.
3. Dufourc, E. J., S. Buchoux, …, B. Odaert. 2012. Membrane interacting peptides: from killers to helpers. *Curr. Protein Pept. Sci.* 13:620–631.
4. Galdiero, S., A. Falanga, …, M. Galdiero. 2013. Peptide-lipid interactions: experiments and applications. *Int. J. Mol. Sci.* 14:18758–18789.
5. Reddy, K. V., R. D. Yedery, and C. Aranha. 2004. Antimicrobial peptides: premises and promises. *Int. J. Antimicrob. Agents.* 24:536–547.
6. Bahar, A. A., and D. Ren. 2013. Antimicrobial peptides. *Pharmaceuticals (Basel).* 6:1543–1575.
7. Melo, M. N., R. Ferre, and M. A. Castanho. 2009. Antimicrobial peptides: linking partition, activity and high membrane-bound concentrations. *Nat. Rev. Microbiol.* 7:245–250.
8. Nguyen, L. T., E. F. Haney, and H. J. Vogel. 2011. The expanding scope of antimicrobial peptide structures and their modes of action. *Trends Biotechnol.* 29:464–472.
9. Bandyopadhyay, S., M. Lee, …, C. Chatterjee. 2013. Model membrane interaction and DNA-binding of antimicrobial peptide Lasioglossin II derived from bee venom. *Biochem. Biophys. Res. Commun.* 430:1–6.

10. de Paula, V. S., G. Razzera, …, A. P. Valente. 2011. Portrayal of complex dynamic properties of sugarcane defensin 5 by NMR: multiple motions associated with membrane interaction. *Structure.* 19:26–36.
11. Kushibiki, T., M. Kamiya, …, K. Kawano. 2014. Interaction between tachyplesin I, an antimicrobial peptide derived from horseshoe crab, and lipopolysaccharide. *Biochim. Biophys. Acta.* 1844:527–534.
12. Saravanan, R., H. Mohanram, …, S. Bhattacharjya. 2012. Structure, activity and interactions of the cysteine deleted analog of tachyplesin-1 with lipopolysaccharide micelle: mechanistic insights into outer-membrane permeabilization and endotoxin neutralization. *Biochim. Biophys. Acta.* 1818:1613–1624.
13. Schibli, D. J., P. M. Hwang, and H. J. Vogel. 1999. Structure of the antimicrobial peptide tritrpticin bound to micelles: a distinct membrane-bound peptide fold. *Biochemistry.* 38:16749–16755.
14. Schibli, D. J., R. F. Epand, …, R. M. Epand. 2002. Tryptophan-rich antimicrobial peptides: comparative properties and membrane interactions. *Biochem. Cell Biol.* 80:667–677.
15. de Medeiros, L. N., R. Angeli, …, F. C. L. Almeida. 2010. Backbone dynamics of the antifungal Psd1 pea defensin and its correlation with membrane interaction by NMR spectroscopy. *Biochim. Biophys. Acta.* 1798:105–113.
16. Feng, J., W. Wang, …, Z. Yuan. 2011. Effects of oligopeptide's conformational changes on its adsorption. *Colloids Surf. B Biointerfaces.* 83:229–236.
17. Bozelli, J. C., Jr., E. T. Sasahara, …, S. Schreier. 2012. Effect of head group and curvature on binding of the antimicrobial peptide tritrpticin to lipid membranes. *Chem. Phys. Lipids.* 165:365–373.
18. Liu, L., Y. Fang, and J. Wu. 2013. Flexibility is a mechanical determinant of antimicrobial activity for amphipathic cationic α-helical antimicrobial peptides. *Biochim. Biophys. Acta.* 1828:2479–2486.
19. Manzini, M. C., K. R. Perez, …, I. M. Cuccovia. 2014. Peptide:lipid ratio and membrane surface charge determine the mechanism of action of the antimicrobial peptide BP100. Conformational and functional studies. *Biochim. Biophys. Acta.* 1838:1985–1999.
20. Respondek, M., T. Madl, …, K. Zangger. 2007. Mapping the orientation of helices in micelle-bound peptides by paramagnetic relaxation waves. *J. Am. Chem. Soc.* 129:5228–5234.
21. Yu, H. Y., B. S. Yip, …, J. W. Cheng. 2013. Correlations between membrane immersion depth, orientation, and salt-resistance of tryptophan-rich antimicrobial peptides. *Biochim. Biophys. Acta.* 1828:2720–2728.
22. Valente, A. P., V. S. de Paula, and F. C. L. Almeida. 2013. Revealing the properties of plant defensins through dynamics. *Molecules.* 18:11311–11326.
23. Oliver, R. C., J. Lipfert, …, L. Columbus. 2013. Dependence of micelle size and shape on detergent alkyl chain length and head group. *PLoS One.* 8:e62488.
24. Pambou, E., J. Crewe, …, J. R. Lu. 2015. Structural features of micelles of zwitterionic dodecyl phosphocholine (C_{12}PC) surfactants studies by small-angle neutron scattering. *Langmuir.* 31:9781–9789.
25. Yang, S. T., S. Y. Yub Shin, …, J. I. Kim. 2002. Conformation-dependent antibiotic activity of tritrpticin, a cathelicidin-derived antimicrobial peptide. *Biochem. Biophys. Res. Commun.* 296:1044–1050.
26. Nagpal, S., V. Gupta, …, D. M. Salunke. 1999. Structure-function analysis of tritrypticin, an antibacterial peptide of innate immune origin. *J. Biol. Chem.* 274:23296–23304.
27. Chan, D. I., E. J. Prenner, and H. J. Vogel. 2006. Tryptophan- and arginine-rich antimicrobial peptides: structures and mechanisms of action. *Biochim. Biophys. Acta.* 1758:1184–1202.
28. Schibli, D. J., L. T. Nguyen, …, H. J. Vogel. 2006. Structure-function analysis of tritrpticin analogs: potential relationships between antimicrobial activities, model membrane interactions, and their micelle-bound NMR structures. *Biophys. J.* 91:4413–4426.
29. Arias, M., K. V. Jensen, …, H. J. Vogel. 2015. Hydroxy-tryptophan containing derivatives of tritrpticin: modification of antimicrobial activity and membrane interactions. *Biochim. Biophys. Acta.* 1848 (1 Pt B):277–288.
30. Salay, L. C., J. Procopio, …, S. Schreier. 2004. Ion channel-like activity of the antimicrobial peptide tritrpticin in planar lipid bilayers. *FEBS Lett.* 565:171–175.
31. Salay, L. C., M. Ferreira, …, S. Schreier. 2012. Headgroup specificity for the interaction of the antimicrobial peptide tritrpticin with phospholipid Langmuir monolayers. *Colloids Surf. B Biointerfaces.* 100:95–102.
32. Lorber, B., J. B. Bishop, and L. J. DeLucas. 1990. Purification of octyl β-D-glucopyranoside and re-estimation of its micellar size. *Biochim. Biophys. Acta.* 1023:254–265.
33. Chevalier, Y., Y. Storet, …, P. Le Perchec. 1991. Tensioactive properties of zwitterionic carboxybetaine amphiphiles. *Langmuir.* 7:848–853.
34. le Maire, M., P. Champeil, and J. V. Moller. 2000. Interaction of membrane proteins and lipids with solubilizing detergents. *Biochim. Biophys. Acta.* 1508:86–111.
35. Stangl, M., A. Veerappan, …, D. Schneider. 2012. Detergent properties influence the stability of the glycophorin A transmembrane helix dimer in lysophosphatidylcholine micelles. *Biophys. J.* 103:2455–2464.
36. Merrifield, R. B. 1963. Solid phase peptide synthesis. I. The synthesis of a tetrapeptide. *J. Am. Chem. Soc.* 85:2149–2154.
37. Amblard, M., J.-A. Fehrentz, …, G. Subra. 2006. Methods and protocols of modern solid phase Peptide synthesis. *Mol. Biotechnol.* 33:239–254.
38. Chan, W., and P. White. 2000. Fmoc Solid Phase Peptide Synthesis. Oxford University Press, New York.
39. Delaglio, F., S. Grzesiek, …, A. Bax. 1995. NMRPipe: a multidimensional spectral processing system based on UNIX pipes. *J. Biomol. NMR.* 6:277–293.
40. Johnson, B. A., and R. A. Blevins. 1994. NMR View: A computer program for the visualization and analysis of NMR data. *J. Biomol. NMR.* 4:603–614.
41. Wüthrich, K. 1990. Protein structure determination in solution by NMR spectroscopy. *J. Biol. Chem.* 265:22059–22062.
42. Lakowicz, J. 2006. Principles of Fluorescence Spectroscopy, 3rd ed. Springer, New York.
43. Anthis, N. J., and G. M. Clore. 2015. Visualizing transient dark states by NMR spectroscopy. *Q. Rev. Biophys.* 48:35–116.
44. Nguyen, L. T., L. de Boer, …, H. J. Vogel. 2011. Investigating the cationic side chains of the antimicrobial peptide tritrpticin: hydrogen bonding properties govern its membrane-disruptive activities. *Biochim. Biophys. Acta.* 1808:2297–2303.
45. Lauterwein, J., C. Bösch, …, K. Wüthrich. 1979. Physicochemical studies of the protein-lipid interactions in melittin-containing micelles. *Biochim. Biophys. Acta.* 556:244–264.
46. Wishart, D. S. 2011. Interpreting protein chemical shift data. *Prog. Nucl. Magn. Reson. Spectrosc.* 58:62–87.
47. He, L., V. M. Garamusm, …, B. Niemeyer. 2002. Comparison of small-angle scattering methods for the structural analysis of octyl-β-maltopyranoside micelles. *J. Phys. Chem. B.* 106:7596–7604.
48. Vitiello, G., D. Ciccarelli, …, G. D'Errico. 2009. Microstructural characterization of lysophosphatidylcholine micellar aggregates: the structural basis for their use as biomembrane mimics. *J. Colloid Interface Sci.* 336:827–833.
49. Stafford, R. E., T. Fanni, and E. A. Dennis. 1989. Interfacial properties and critical micelle concentration of lysophospholipids. *Biochemistry.* 28:5113–5120.
50. Palladino, P., F. Rossi, and R. Ragone. 2010. Effective critical micellar concentration of a zwitterionic detergent: a fluorimetric study on *n*-dodecyl phosphocholine. *J. Fluoresc.* 20:191–196.
51. McLachlan, A. A., and D. G. Marangoni. 2006. Interactions between zwitterionic and conventional anionic and cationic surfactants. *J. Colloid Interface Sci.* 295:243–248.
52. Nussinov, R., B. Ma, and C.-J. Tsai. 2014. Multiple conformational selection and induced fit events take place in allosteric propagation. *Biophys. Chem.* 186:22–30.

53. Wang, Q., P. Zhang, …, M. S. Cheung. 2013. Protein recognition and selection through conformational and mutually induced fit. *Proc. Natl. Acad. Sci. USA.* 110:20545–20550.

54. Monod, J., J. Wyman, and J.-P. Changeux. 1965. On the nature of allosteric transitions: a plausible model. *J. Mol. Biol.* 12:88–118.

55. Henzler-Wildman, K., and D. Kern. 2007. Dynamic personalities of proteins. *Nature.* 450:964–972.

56. Boehr, D. D., R. Nussinov, and P. E. Wright. 2009. The role of dynamic conformational ensembles in biomolecular recognition. *Nat. Chem. Biol.* 5:789–796.

57. Warschawski, D. E., A. A. Arnold, …, I. Marcotte. 2011. Choosing membrane mimetics for NMR structural studies of transmembrane proteins. *Biochim. Biophys. Acta.* 1808:1957–1974.

58. Hocking, H. G., K. Zangger, and T. Madl. 2013. Studying the structure and dynamics of biomolecules by using soluble paramagnetic probes. *ChemPhysChem.* 14:3082–3094.

59. Andrushchenko, V. V., M. H. Aarabi, …, H. J. Vogel. 2008. Thermodynamics of the interactions of tryptophan-rich cathelicidin antimicrobial peptides with model and natural membranes. *Biochim. Biophys. Acta.* 1778:1004–1014.

60. Changeux, J.-P., and S. Edelstein. 2011. Conformational selection or induced fit? 50 years of debate resolved. *F1000 Biol. Rep.* 3:19–34.

61. Koshland, D. E. 1958. Application of a theory of enzyme specificity to protein synthesis. *Proc. Natl. Acad. Sci. USA.* 44:98–104.

62. Koshland, D. E., Jr., G. Némethy, and D. Filmer. 1966. Comparison of experimental binding data and theoretical models in proteins containing subunits. *Biochemistry.* 5:365–385.

63. Aleksandrov, A., and T. Simonson. 2010. Molecular dynamics simulations show that conformational selection governs the binding preferences of imatinib for several tyrosine kinases. *J. Biol. Chem.* 285:13807–13815.

64. Fenwick, R. B., S. Esteban-Martín, and X. Salvatella. 2011. Understanding biomolecular motion, recognition, and allostery by use of conformational ensembles. *Eur. Biophys. J.* 40:1339–1355.

65. Feixas, F., S. Lindert, …, J. A. McCammon. 2014. Exploring the role of receptor flexibility in structure-based drug discovery. *Biophys. Chem.* 186:31–45.

66. Grünberg, R., J. Leckner, and M. Nilges. 2004. Complementarity of structure ensembles in protein-protein binding. *Structure.* 12:2125–2136.

67. Wlodarski, T., and B. Zagrovic. 2009. Conformational selection and induced fit mechanism underlie specificity in noncovalent interactions with ubiquitin. *Proc. Natl. Acad. Sci. USA.* 106:19346–19351.

68. Benfield, A. P., M. G. Teresk, …, S. F. Martin. 2006. Ligand preorganization may be accompanied by entropic penalties in protein-ligand interactions. *Angew. Chem. Int. Ed. Engl.* 45:6830–6835.

69. Blundell, C. D., M. J. Packer, and A. Almond. 2013. Quantification of free ligand conformational preferences by NMR and their relationship to the bioactive conformation. *Bioorg. Med. Chem.* 21:4976–4987.

70. Arias, M., E. R. Hoffarth, …, H. J. Vogel. 2016. Recombinant expression, antimicrobial activity and mechanism of action of tritrpticin analogs containing fluoro-tryptophan residues. *Biochim. Biophys. Acta.* 1858:1012–1023.

71. Bourbigot, S., E. Dodd, …, V. Booth. 2009. Antimicrobial peptide RP-1 structure and interactions with anionic versus zwitterionic micelles. *Biopolymers.* 91:1–13.

72. Tinoco, L. W., F. Gomes-Neto, …, F. C. L. Almeida. 2007. Effect of micelle interface on the binding of anticoccidial PW2 peptide. *J. Biomol. NMR.* 39:315–322.

73. Cruzeiro-Silva, C., F. Gomes-Neto, …, A. P. Valente. 2007. Structural biology of membrane-acting peptides: conformational plasticity of anticoccidial peptide PW2 probed by solution NMR. *Biochim. Biophys. Acta.* 1768:3182–3192.

74. de Planque, M. R., B. B. Bonev, …, J. A. Killian. 2003. Interfacial anchor properties of tryptophan residues in transmembrane peptides can dominate over hydrophobic matching effects in peptide-lipid interactions. *Biochemistry.* 42:5341–5348.

75. Norman, K. E., and H. Nymeyer. 2006. Indole localization in lipid membranes revealed by molecular simulation. *Biophys. J.* 91:2046–2054.

76. de Jesus, A. J., and T. W. Allen. 2013. The role of tryptophan side chains in membrane protein anchoring and hydrophobic mismatch. *Biochim. Biophys. Acta.* 1828:864–876.

77. Yau, W. M., W. C. Wimley, …, S. H. White. 1998. The preference of tryptophan for membrane interfaces. *Biochemistry.* 37:14713–14718.

78. Haney, E. F., S. Nathoo, …, E. J. Prenner. 2010. Induction of non-lamellar lipid phases by antimicrobial peptides: a potential link to mode of action. *Chem. Phys. Lipids.* 163:82–93.

79. Koller, D., and K. Lohner. 2014. The role of spontaneous lipid curvature in the interaction of interfacially active peptides with membranes. *Biochim. Biophys. Acta.* 1838:2250–2259.

Biophysical Journal, Volume *111*

Supplemental Information

Structural and Dynamic Insights of the Interaction between Tritrpticin and Micelles: An NMR Study

Talita L. Santos, Adolfo Moraes, Clovis R. Nakaie, Fabio C.L. Almeida, Shirley Schreier, and Ana Paula Valente

SUPPORTING MATERIAL

Structural and dynamic insights of the interaction between the antimicrobial peptide tritrpticin and micellar interfaces – an NMR study

Running Title: NMR study of tritrpticin-micelle interaction

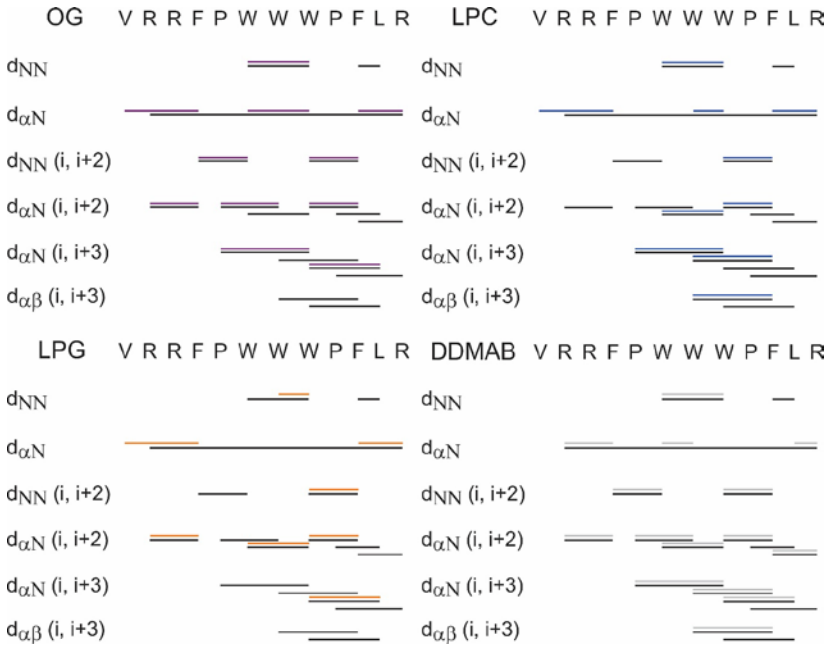

Figure S1. Sequential and medium range NOEs for TRP3 in 50 mM OG (purple), 13.5 mM LLPC (blue), 15 mM LMPG (orange), 30 mM DDMAB (gray), and 100 mM DPC (black). The results for DPC were used for comparison with the other micelles. TRP3 showed helical propensity in all systems, as well as similar conformations.

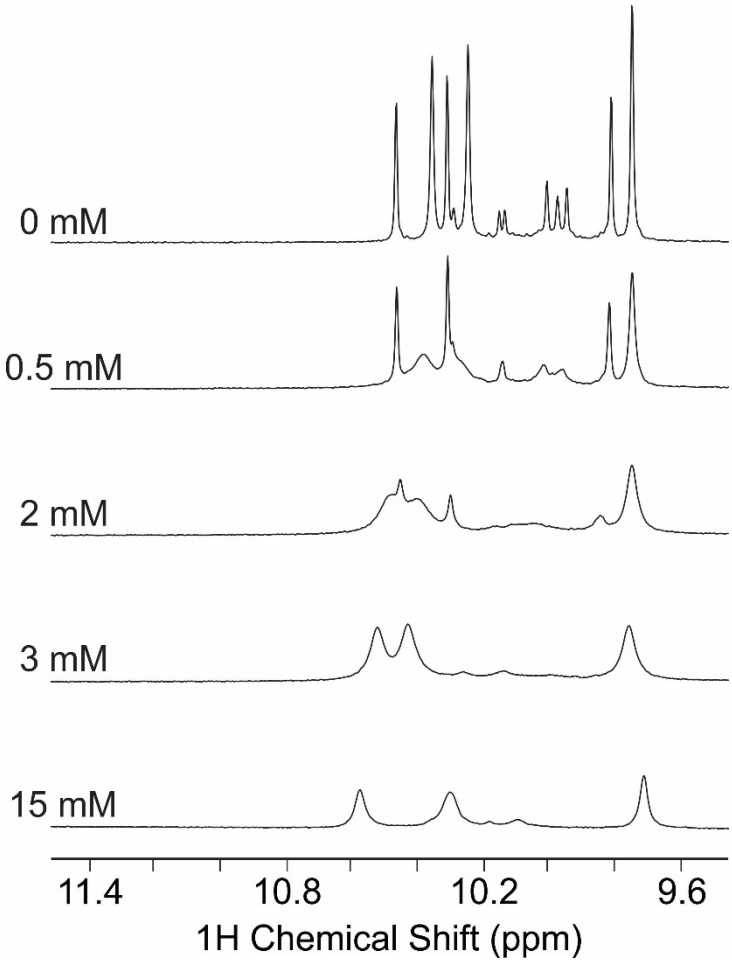

Figure S2. NH indole region of TRP3 1D-NMR spectra in the presence of increasing LMPG concentrations, without intensity normalization.

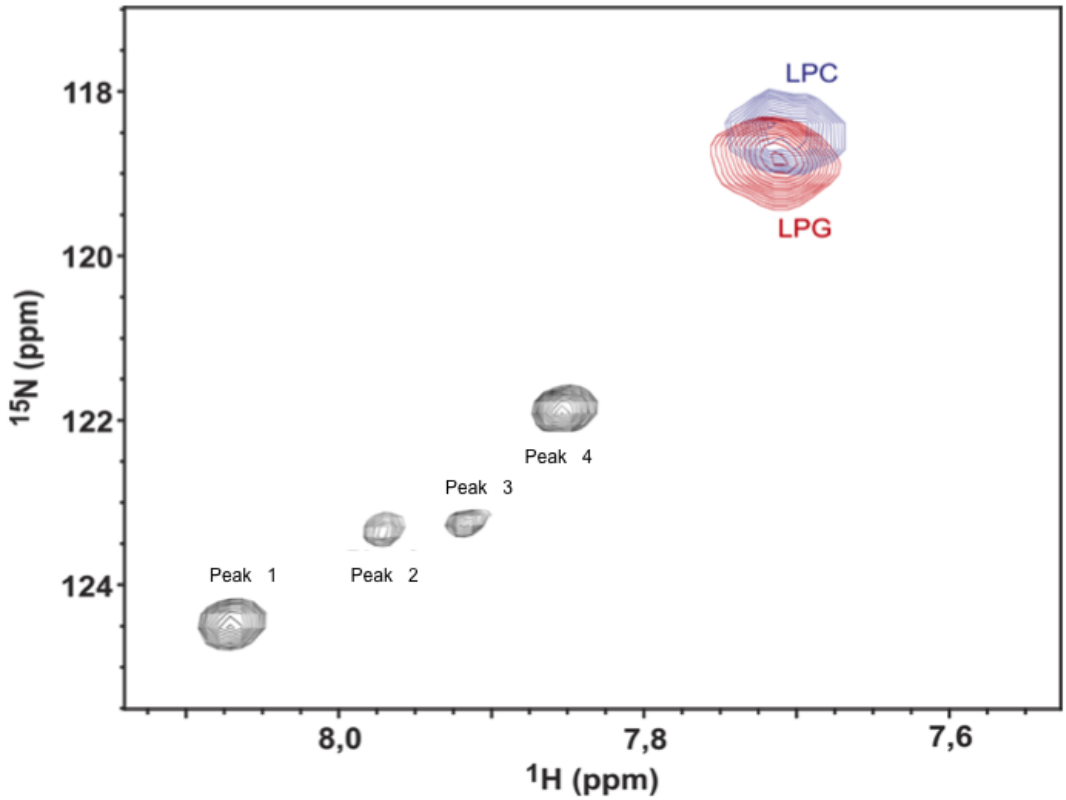

Figure S3. ^{1}H-^{15}N HSQC of TRP3 in the absence and presence of 13.5 mM LLPC or 15 mM LMPG. In absence of micelles, TRP3 presents four peaks for ^{15}N-L[11].

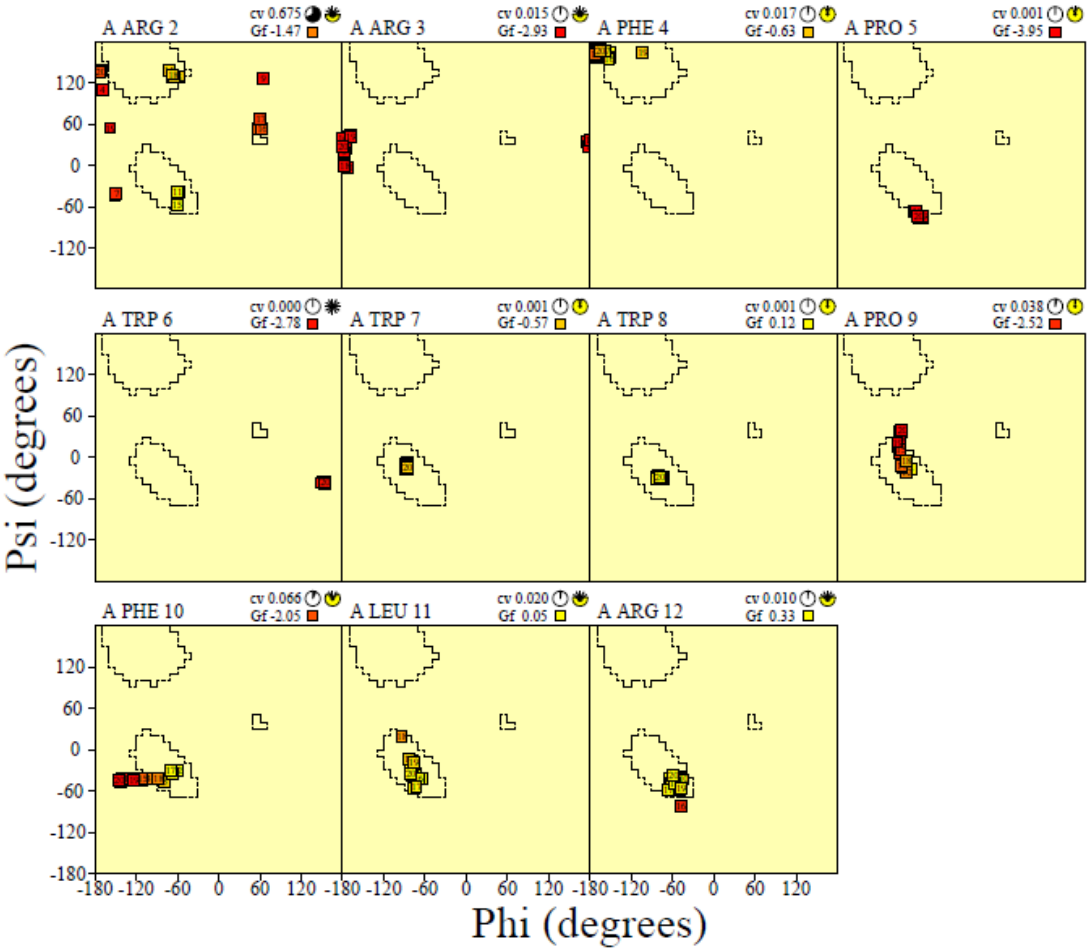

Figure S4. Ramachandran Plot of TRP3 in DPC micelles (PDB: 2I1D). Note that most of the residues (mainly the F4-L11 stretch) are in a helical region.

TABLE S1. TRP3 ^{15}N-L^{11} relaxation and rotational correlation times, in the absence or presence of micelles.

	T_1 (ms)	T_2 (ms)	Het-NOE	τ_c(ns)[b]
Peak 1[a]	680 ± 32	390 ± 19	0.46 ± 0.02	2.1
Peak 2[a]	715 ± 34	404 ± 20	0.59 ± 0.03	2.1
Peak 3[a]	777 ± 38	477 ± 22	0.54 ± 0.03	1.9
Peak 4[a]	638 ± 30	398 ± 20	0.21 ± 0.01	1.8
LLPC	1120 ± 60	40.5 ± 2	0.56 ± 0.03	14.1
LMPG	1009 ± 50	30.8 ± 2	0.61 ± 0.03	15.4

[a]TRP3 Peaks found in solution; [b]Rotational correlation time estimated using relaxation parameters.

TABLE S2. TRP3 PRE obtained information[a] in the presence of micelles.

	τ^1		ρ^2		Depth (Å)
LLPC	-0.73 ± 0.02	-41.8 ± 1.2°	-1.05 ± 0.04	-56.8 ± 2.7°	-1.07 ± 0.3
LMPG	-0.62 ± 0.06	-35.5 ± 3.5°	-0.99 ± 0.05	-60.3 ± 2.2°	-2.62 ± 0.2

[a]Angles (rad and deg) between F4 and L11: [1]tilt and [2]azimuth angles.